Kinetic modeling study of the laser-induced plasma plume of cyclotrimethylenetrinitramine (RDX) ☆

V.I. Babushok [a,*], F.C. DeLucia Jr. [b], P.J. Dagdigian [c], J.L. Gottfried [b], C.A. Munson [b], M.J. Nusca [b], A.W. Miziolek [b]

[a] National Institutes of Standards and Technology, Gaithersburg, MD 20899, USA
[b] U.S. Army Research Laboratory, AMSRL-WM-BD, Aberdeen Proving Ground, MD 21005-5069, USA
[c] Department of Chemistry, The Johns Hopkins University, Baltimore, MD 21218-2685, USA

Abstract

A kinetic model of a laser-induced breakdown spectroscopy (LIBS) plume of cyclotrimethylenetrinitramine (RDX) was developed for the analysis of processes responsible for the LIBS signature of explosives. Air and argon were considered as buffer gases. The model includes a set of processes involving ion chemistry, as well as excitation, ionization, and other processes affecting neutral and ion species. Modeling results show that the overall reaction process can be considered a two-stage process. The first stage corresponds to a fast approach to a quasi-stationary state, while the second stage corresponds to the change of quasi-stationary species concentrations due to the change in temperature. As a result of the two-stage process, the initial mechanism of explosive decomposition is not important in determining its signature in the LIBS measurement time window (1–30 μs). The main processes responsible for generation of excited states for the LIBS emission are electron-excitation impact processes. A mechanism for the appearance of a double peak of the C_2 species concentration in the RDX plasma plume was suggested. Double-peak behavior of the C_2 species was previously experimentally observed during laser ablation of graphite.
Published by Elsevier B.V.

Keywords: Laser-induced breakdown spectroscopy; Laser plasma; Kinetic model; RDX; Explosive

1. Introduction

Laser-induced breakdown spectroscopy (LIBS) is an emerging diagnostic method for many applications. A LIBS operates with a high power laser pulse focused on small spot of a sample material. The interaction of the pulsed laser beam with a sample material produces high-temperature ionized plasma containing electronically excited elements which radiate the characteristic emission lines of corresponding elements. It is important to note that the laser energy release time occurs in the femtosecond–nanosecond temporal range. However a plasma kernel with high temperature exists for 10–100 μs, as a result of chemical reactions and recombination processes, releasing energy on the microsecond time scale and sustaining the plasma.

The direct detection of energetic materials and explosives in real time is an important practical problem [1–3]. The LIBS technique is mainly considered to be a method of analytical element analysis. However, the LIBS technique allows one to identify certain chemical compounds with chemometric analysis. Results of recent LIBS studies of energetic materials demonstrate that the simultaneous registration O, N, H and C_2 signals [1–3] and analysis of the ratios of peak intensities allows one to make definite conclusions on the presence of energetic material.

The aim of the present work was to develop a kinetic model of the LIBS plume of RDX for the analysis of processes responsible for the RDX LIBS signature. RDX (1,3,5-trinitrohexahydro-s-triazine) is an explosive nitroamine widely used in military and

Report Documentation Page		*Form Approved* *OMB No. 0704-0188*

Public reporting burden for the collection of information is estimated to average 1 hour per response, including the time for reviewing instructions, searching existing data sources, gathering and maintaining the data needed, and completing and reviewing the collection of information. Send comments regarding this burden estimate or any other aspect of this collection of information, including suggestions for reducing this burden, to Washington Headquarters Services, Directorate for Information Operations and Reports, 1215 Jefferson Davis Highway, Suite 1204, Arlington VA 22202-4302. Respondents should be aware that notwithstanding any other provision of law, no person shall be subject to a penalty for failing to comply with a collection of information if it does not display a currently valid OMB control number.

1. REPORT DATE **2007**	2. REPORT TYPE	3. DATES COVERED **00-00-2007 to 00-00-2007**

4. TITLE AND SUBTITLE **Kinetic modeling study of the laser-induced plasma plume of cyclotrimethylenetrinitramine (RDX)**	5a. CONTRACT NUMBER **W911NF-06-1-0446**
	5b. GRANT NUMBER
	5c. PROGRAM ELEMENT NUMBER

6. AUTHOR(S)	5d. PROJECT NUMBER
	5e. TASK NUMBER
	5f. WORK UNIT NUMBER

7. PERFORMING ORGANIZATION NAME(S) AND ADDRESS(ES) **National Institutes of Standards and Technology,Gaithersburg,MD,20899**	8. PERFORMING ORGANIZATION REPORT NUMBER **; 50351.1**

9. SPONSORING/MONITORING AGENCY NAME(S) AND ADDRESS(ES) **U.S. Army Research Office, P.O. Box 12211, Research Triangle Park, NC, 27709-2211**	10. SPONSOR/MONITOR'S ACRONYM(S)
	11. SPONSOR/MONITOR'S REPORT NUMBER(S) **50351.1**

12. DISTRIBUTION/AVAILABILITY STATEMENT **Approved for public release; distribution unlimited**

13. SUPPLEMENTARY NOTES

14. ABSTRACT

15. SUBJECT TERMS

16. SECURITY CLASSIFICATION OF:			17. LIMITATION OF ABSTRACT	18. NUMBER OF PAGES	19a. NAME OF RESPONSIBLE PERSON
a. REPORT **unclassified**	b. ABSTRACT **unclassified**	c. THIS PAGE **unclassified**	**Same as Report (SAR)**	**8**	

Standard Form 298 (Rev. 8-98)
Prescribed by ANSI Std Z39-18

industrial applications. It is considered one of the most powerful military explosives. The developed model includes processes of formation and quenching of excited H, N and O atoms, and a submodel for formation of the C_2 molecule. The observation of LIBS C_2 signals was used to discriminate organic samples from inorganic targets during detection of energetic materials [2]. Together with peak ratios, the data on C_2 emission was used for the detection of a number of explosive materials. In future studies, we plan to reduce suitably the developed model for detailed CFD modeling studies of RDX LIBS plume. The results of the present kinetic modeling suggest that the assembled model can be used for understanding the reaction behavior in the LIBS plume of other C/H/N/O-containing explosive materials.

2. Kinetic model

As the first step in the analysis of processes responsible for the emission lines in the plasma plume of explosives, a kinetic model of RDX reaction behavior in the LIBS plume was developed. Air and argon were considered as buffer gases. Earlier we developed a kinetic model of lead reactions in air and argon [4,5] to describe the chemical reactions and collisional processes that occur within the high-temperature mixture in the LIBS plume. These processes were included as a part of the current model. The model includes a set of processes involving ion chemistry, as well as excitation, ionization, and other processes affecting neutral and ion species.

The kinetic model of RDX reactions in the plume includes the following main reaction subsets: RDX decomposition reactions, high-temperature air and argon plasma reactions of neutral species, reactions of ionization and reactions of charged

Table 1
States of atomic nitrogen, hydrogen and oxygen included in the kinetic model

Atom	Level	Energy, cm^{-1}	Emission line, nm
N	2p^3 ^{4}S^0	0	(L)520,347,120,113.4
N*2	2p^3 ^{2}D^0	19,226	(U)520,(L)149
N*3	2p^3 ^{2}P^0	28,839	(U)347,(L)175
N*4	2p^{2}3s ^{4}P	83,337	(U)120,(L)(870),(821),747,742
N*5	2p^{2}3s ^{2}P	86,192	(U)149,175,(L)135,947,(940),742.861
N*6	2s^{2}2p^4 ^{4}P	88,134	(U)113
N*7	2p^{2}3p ^{2}S^0	93,582	(L) 947,939,(857–866)
N*8	2p^{2}3p ^{4}D^0	94,839	(U)(868–874)
N*9	2p^{2}3p ^{4}P^0	95,511	(U)821
N*10	2p^{2}3p ^{4}S^0	96,752	(U)745,947
N*11	2p^{2}3p ^{2}D^0	96,834	(U)740.9,939.5
N*12	2p^{2}3p ^{2}P^0	97,793	(U)861
O	2p^4 ^{3}P	0	
O*2	2p^4 ^{1}D	15,865	
O*3	2p^4 ^{1}S	33,795	
O*4	3s ^{5}S^0	73,769	(L)777
O*5	3s ^{3}S^0	76,794	(L)844
O*6	3p ^{5}P	86,626	(U)777
O*7	3p ^{3}P	88,642	(U)844
O*8	4s ^{5}S^0	95,498	
H	$n=1$	0	(L)102.5, 121.6
H*2	$n=2$	82,259	(L)656,(U)102.5
H*3	$n=3$	97,492	(U)121.6, 656

Table 2
Kinetic models of RDX decomposition used in this work

Kinetic model	Model details
Gas-phase decomposition model	Model of initial RDX decomposition of Chakraborthy et al. [8]
Initial gas composition on the surface from RDX decomposition and detailed gas-phase model of this work	Decomposition products at the surface, experimental data of Fetherolf and Litzinger [11]
Two overall subsurface reactions and gas-phase mechanism of this work	Subsurface decomposition model from [12]
Overall reaction of decomposition and detailed mechanism of this work	Overall decomposition reaction from [10]

species (e−, H$^+$, O$^+$, O$_2^+$, N$^+$, NO$^+$, N$_2^+$, H$_2^+$, OH$^+$, H$_2$O$^+$, O$_2^-$, O$^-$, C$^+$, CO$^+$, CO$_2^+$, CH$_3^+$, CH$_4^+$, CH$^+$, CH$_2^+$, C$_2$H$_3^+$, C$_2$H$_2^+$, N$_4^+$, N$_2$O$_2^+$, N$_3$O$^+$, N$_2$O$^+$, N$_3^+$, NO$_2^+$, NO$_3^+$, NO$^-$, N$_2$O$^-$, NO$_2^-$, NO$_3^-$), reactions generating the electronically excited atoms N, O, and H and their reactions in the plasma plume. Table 1 contains the electronic states of atomic N, O, and H included in the model. For example, the following excited states of the oxygen atom were included in the kinetic model: ground state O(^{3}P), two metastable states O(^{1}D) and O(^{1}S) and excited states 3s ^{5}S, 3s ^{3}S, 3p ^{5}P, and 3p ^{3}P, which participate in the 777 nm and 844 nm O atom transitions.

Thus the model includes the following reaction subsets:
1. Initial decomposition reactions of RDX (or explosive products at the surface of target material)
2. High-temperature reactions of products of explosive decomposition in the buffer gas under the LIBS conditions (buffer gas: Ar or air).
3. Reactions of excited states species responsible for the LIBS signature, including the generation and quenching of excited states (O, H, N) and the subset of reactions of excited species with the decomposition products of RDX and with buffer gas species.

The kinetic model was assembled from several sources. Main sources of data are identified below. When absent, kinetic data were estimated based on analogy or with the use of empirical rules. The kinetic model contains overall 137 species, with 577 reactions. To describe RDX decomposition, several mechanisms were used [6–10] (Table 2). A plasma kinetic model for the H/N/O/Ar system was taken from our previous work [4,5]. Plasma chemistry reactions related to the C/H/O/N system came from several sources [13–15]. Reactions involving the C_2 species were added on the basis of the results of Kruse and Ross [16,17]. Kinetic data for electronically excited O, H and N atoms (electron-impact excitation cross sections, radiative quenching rates, etc) were taken from [18−21]. Table 3 contains the block of reactions describing the kinetics of C_2 formation and consumption, and a block of ion reactions involving carbon-containing species. The kinetic submodel describing the formation and decay of electronically excited H, N and O atoms will be presented in a separate publication. Note that the kinetic model doesn't currently include excited C atom states. The excited states of carbon atom will be considered in a future work.

Of course, at these high temperatures, a large number of rate constant values was obtained by extrapolation from rate

Table 3

Reactions of C_2 formation and carbon-containing ions [the rate constant k (cm, s, mol units) is expressed in the Chemkin format as $AT^n \exp(-E/RT)$]

No Reaction	A(mole, cm, s)	n	E(cal/mole)	Reference
Reactions of C_2 formation				
1. $C_2+M=C+C+M$	1.50E+16	0.0	142,400.0	[17]
2. $C_2+H_2=C_2H+H$	6.60E+13	0.0	8000.0	[17]
3. $C_2H+M=C_2+H+M$	1.74E+35	−5.16	114,000.0	[17]
4. $C_2H+C_2H=C_2H_2+C_2$	1.80E+12	0.0	0.0	[22]
5. $CN+C=C_2+N$	3.00E+14	0.0	35,968.0	[23]
6. $C_2+N_2=CN+CN$	6.40E+11	0.0	24,900.0	[16]
7. $C_2+N_2=C_2N+N$	3.30E+14	0.0	67,660.0	[16]
8. $C_2+C_2=C_3+C$	3.20E+14	0.0	0.0	[17]
9. $H+CH=C+H_2$	1.10E+14	0.0	0.0	[8]
10. $C+C_2H=C_3+H$	7.00E+14	0.0	0.0	[17]
11. $C_2+CH=C_3+H$	2.00E+14	0.0	0.0	[17]
12. $CH+CH=C_2+H+H$	1.00E+14	0.0	0.0	[17]
13. $CH+CH=C_2H_2$	1.20E+14	0.0	0.0	[14]
14. $C_3H+H=C_3+H_2$	1.00E+14	0.0	0.0	[17]
15. $C_3H_2+H=C_3H+H_2$	6.31E+13	0.0	0.0	[17]
16. $C_3+M=C_2+C+M$	4.00E+16	0.0	150,000.0	[17]
17. $CH+M=C+H+M$	1.90E+14	0.0	66,968.0	[17]
18. $CH_2+M=C+H_2+M$	1.15E+14	0.0	55,820.0	[17]
19. $CH_2+M=CH+H+M$	2.88E+14	0.0	79,030.0	[17]
20. $C_3H+M=C_3+H+M$	1.58E+14	0.0	39,420.0	[17]
21. $C_3H_2+M=C_3H+H+M$	1.00E+15	0.0	60,000.0	[17]
22. $C_2+O=CO+C$	7.60E+14	0.0	12,380.0	[17]
23. $NO+C_2=C_2N+O$	4.70E+13	0.0	8644.0	[16]
24. $NO+C_2=C_2O+N$	2.80E+13	0.0	8644.0	[16]
25. $C_3+O=CO+C_2$	3.00E+14	0.0	0.0	[16]
26. $C_3+O=C_2O+C$	1.00E+14	0.0	0.0	[16]
27. $C+NO=CN+O$	1.90E+13	0.0	0.0	[8]
28. $C+NO=CO+N$	2.90E+13	0.0	0.0	[8]
29. $C+N_2=CN+N$	6.30E+13	0.0	46,020.0	[8]
30. $CN+NO=NCO+N$	9.64E+13	0.0	42,130.0	[16]
31. $CN+NO=N_2+CO$	2.51E+10	0.0	0.0	[16]
32. $CN+M=C+N+M$	2.50E+14	0.0	141,010.0	[16]
33. $C_2N+N=CN+CN$	6.03E+13	0.0	0.0	[16]
34. $C_2N+O=C_2O+N$	1.00E+14	0.0	0.0	[16]
35. $C_2N+M=CN+C+M$	1.00E+16	0.0	130,000.0	[16]
36. $C+CO+M=C_2O+M$	2.29E+16	0.0	0.0	[16]
37. $CN+O=CO+N$	7.70E+13	0.0	0.0	[8]
38. $CN+H_2=HCN+H$	2.10E+13	0.0	4710.00	[8]
39. $O_2+C_2=CO+CO$	6.60E+12	0.0	757.0	[24]
40. $OH+C_2=CO+CH$	5.00E+12	0.0	0.0	[25]
41. $CN+CO_2=NCO+CO$	4.00E+14	0.0	38,400.0	[26]
42. $CN+CO=NCO+C$	1.50E+16	−0.487	131,600.0	[26]
43. $CO+O \Rightarrow CO_2$ (radiative recombination)	2.50E+06	0.0	3200.0	[15]
44. $CO_2+C=CO+CO$	6.00E+08	0.0	0.0	[15]
45. $C+O+M=CO+M$	7.26E+13	0.0	0.0	[27]
46. $OH+C=H+CO$	5.00E+13	0.0	0.0	[8]
47. $C+O_2=O+CO$	5.80E+13	0.0	576.0	[8]
48. $C+CH_2=H+C_2H$	5.00E+13	0.0	0.0	[8]
49. $C+CH_3=H+C_2H_2$	5.00E+13	0.0	0.0	[8]
50. $C+N_2=CN+N$	6.30E+13	0.0	46,020.0	[8]
Reactions of C-containing ions				
1. $C+O=E+CO^+$	8.80E+08	1.0	66,200.0	[26]
2. $NO^++C=NO+C^+$	1.00E+13	0.0	46,400.0	[26]
3. $CO+C^+=C+CO^+$	1.00E+13	0.0	62,800.0	[26]
4. $O_2+C^+=C+O_2^+$	1.00E+13	0.0	18,800.0	[26]
5. $C+E=E+E+C^+$	3.90E+33	−3.78	261,400.0	[26]
6. $E+O+\Rightarrow O$ (radiative recombination)	1.07E+11	−0.52	0.0	[26]
7. $E+C+\Rightarrow C$ (radiative recombination)	2.02E+11	−0.46	0.0	[26]

Table 3 (*continued*)

No Reaction	A(mole, cm, s)	n	E(cal/mole)	Reference
Reactions of C-containing ions				
8. $E+CH_3^+=CH+H+H$	4.30E+14	0.5	0.0	[14]
9. $O+NO^+=N+O_2^+$	7.20E+12	0.29	97,200.0	[26]
10. $CH_4+CH_3^+=CH_3+CH_4^+$	8.20E+13	0.0	0.0	[28]
11. $H_2^+CH_2^+=H+CH_3^+$	9.60E+14	0.0	0.0	[28]
12. $H_2+CH^+=H+CH_2^+$	7.20E+14	0.0	0.0	[28]
13. $CH_4+C^+=H+C_2H_3^+$	4.80E+14	0.0	0.0	[28]
14. $CH_4+C^+=H_2+C_2H_2^+$	2.40E+14	0.0	0.0	[28]
15. $C+H^+=H+C^+$	1.80E+15	0.0	0.0	[29]
16. $O+CO^+=CO+O^+$	8.40E+13	0.0	0.0	[29]
17. $E+CO^+=C+O$	1.86E+18	−0.5	0.0	[29]
18. $E+CO=E+E+CO^+$	5.88E+12	0.5	300,000.0	[15]
19. $E+CO=E+E+O+C^+$	1.68E+12	0.5	300,000.0	[15]
20. $E+CO=E+E+C+O^+$	8.40E+11	0.5	300,000.0	[15]
21. $E+CO_2=E+E+CO_2^+$	5.46E+12	0.5	300,000.0	[15]
22. $E+CO_2=E+E+O+CO^+$	8.40E+11	0.5	300,000.0	[15]
23. $E+CO_2=>E+E+O_2+C^+$	8.40E+11	0.5	300,000.0	[15]
24. $E+CO_2=E+E+CO+O^+$	8.40E+11	0.5	300,000.0	[15]
25. $E+CO_2=E+E+C+O_2^+$	4.20E+11	0.5	300,000.0	[15]
26. $CO+E=C+O^-$	1.60E+07	0.0	0.0	[15]
27. $CO_2+E=CO+O^-$	3.00E+11	0.0	0.0	[15]
28. $O+E=O^-$	2.60E+06	0.0	0.0	[15]
29. $O+E+M=O^-+M$	3.60E+16	0.0	−600.0	[15]
30. $CO+AR^+=AR+CO^+$	4.80E+13	0.0	0.0	[15]
31. $C^++NO_2^-=C+NO_2$	1.97E+18	−0.5	0.0	[15]
32. $AR^++NO_2^-=AR+NO_2$	5.00E+19	−0.5	0.0	[15]
33. $AR^++NO_3^-=AR+NO_3$	5.10E+17	−0.5	0.0	[15]
34. $C^++NO_3^-=C+NO_3$	2.00E+18	−0.5	0.0	[15]
35. $CO_2+AR^+=AR+CO_2^+$	4.56E+14	0.0	0.0	[15]
36. $O+AR^+=AR+O^+$	3.84E+12	0.0	0.0	[15]
37. $O_2+AR^+=AR+O_2^+$	2.76E+13	0.0	0.0	[15]
38. $CO_2+C^+=CO+CO^+$	6.60E+14	0.0	0.0	[15]
39. $O_2+C^+=CO+O^+$	3.68E+14	0.0	0.0	[15]
40. $O_2+C^+=O+CO^+$	2.25E+14	0.0	0.0	[15]
41. $CO_2+CO^+=CO+CO_2^+$	6.00E+14	0.0	0.0	[15]
42. $O_2+CO^+=CO+O_2^+$	7.20E+13	0.0	0.0	[15]
43. $O+CO_2^+=CO+O_2^+$	9.80E+13	0.0	0.0	[15]
44. $O+CO_2^+=CO_2+O^+$	5.77E+13	0.0	0.0	[15]
45. $O_2+CO_2^+=CO_2+O_2^+$	3.84E+13	0.0	0.0	[15]
46. $CO_2+O^+=CO+O_2^+$	2.70E+14	0.0	0.0	[15]
47. $CO_2+O^+=O+CO_2^+$	2.70E+14	0.0	0.0	[15]
48. $CO+O^-=CO_2+E$	3.30E+14	0.0	0.0	[15]

constants measured at much lower temperatures (1000–3000 K), appropriate to flames. Some temperature dependencies of rate constants [6–9] were approximated by dependencies, which are valid at flame temperatures. Their extrapolation can lead to erroneous results. The kinetic model was examined for possible incorrect use of extrapolated temperature dependencies of rate constants. Rate constants with large n values (negative or positive) were modified using literature data, where they were available, or were re-scaled.

The Chemkin package [31] was used for kinetic modeling of reaction processes in the plasma plume. Reaction pathway analysis and calculation of sensitivity coefficients were applied to characterize the main reactions and the reaction mechanism in the plasma kernel. Kinetic modeling was performed with parameters which correspond to our experimental conditions (temperature range, cooling rate, times of emission registration). It was assumed that the heating of the gas takes place instantaneously, since the duration of the laser shot and the

Table 4
Time to attain equilibrium at a constant temperature (10 atm, mixture 0.2 O_2 + 0.03 H_2O + 0.77 N_2)

Temperature	Time (model without ionization)	Time (model with ionization)
10,000 K	2×10^{-5}	2×10^{-5}
12,000 K	7×10^{-6}	$\sim 7 \times 10^{-6}$
15,000 K	2.7×10^{-6}	3.5×10^{-6}
20,000 K	2.5×10^{-6}	$\sim 3 \times 10^{-6}$
30,000 K	2.3×10^{-6}	$\sim 3 \times 10^{-6}$

generation of the plasma is short compared with the beginning and duration of the LIBS signal. Assumed initial temperatures were in the range 12,000–20,000 K. These temperatures correspond to experimentally observed temperatures [32,33]. It was assumed that the cooling of the gas follows exponential temperature decay with the characteristic decay times of 2–30 μs, corresponding to experimental measurements and to typical times of LIBS registration of the emission from excited atoms in the plasma kernel [32–34]. Note that in real experimental conditions, pressure is a variable parameter and, for the studied time range, the sample gas will possibly remain largely unmixed with a buffer gas. Nevertheless, even taking into account these more realistic conditions, the underlying features of chemistry and the mechanism of reaction process should remain the same. Below a short discussion will be presented concerning the temperature dependence of reaction rates, reaction times and the level of equilibrium electron densities for LIBS plasma conditions.

2.1. Leveling-off of temperature dependence of reaction rate. Reaction time

It should be noted that temperatures of the order of 15,000 K (and higher), appropriate to LIBS plasmas, actually lead to relatively similar rate constants for different reactions, since the Arrhenius exponential temperature dependence of reaction rates levels off at high temperatures. Thus, the characteristic reaction times for radicals and stable molecules become similar, even with differing activation energies of reaction. Even with a further increase in temperature, a limiting reaction time, e.g. the time

required to attain equilibrium, is observed. Thus a high-temperature decomposition of typical explosives very quickly leads to a set of simple species consisting of N,C,H and O atoms. The largest time of decomposition of species with two or three atoms belongs possibly to the nitrogen molecule. We estimate that the time to attain equilibrium in the N_2 system is 2–4 μs at 15,000 K and 10 atm. The time to reach equilibrium conditions is likely in the μs range, and an increase in temperature should not significantly affect this time. Note that inverse bremsstrahlung and multiphoton ionization processes (which were not considered in this work) will accelerate chemical reaction processes during the initial period. However, the relatively slow reactions will determine the time to attain equilibrium.

Calculated times to attain thermodynamic equilibrium at different temperatures (under constant temperature) are presented in Table 4 for the N/H/O system. The initial gas mixture composition was $0.2O_2 + 0.03H_2O + 0.77N_2$. This composition corresponds to humid air atmosphere and includes gases which are typically found in the products of decomposition of solid explosives. The results may lead to several conclusions. The relatively long time to attain equilibrium suggests that the initial decomposition chemistry of explosives may be of importance in the chemistry of the LIBS plume. Also, it means that the chemistry may influence the concentration level of emitting species, leading to a chemical effect on the LIBS signature. Of course, the temperature and pressure conditions, which affect electronic quenching, are the most important factors in determining the concentration levels of the emitting species. Nevertheless, as it will be demonstrated below, the LIBS plasma loses memory of the initial compound at substantially shorter times in comparison with equilibration times.

In calculations the equilibration time was determined as the time to reach 95% of the equilibrium concentration. The quoted times represent estimates under the assumption of our kinetic model and the rate constants employed in the model.

2.2. Equilibrium electron density in different gases

The importance of electron-impact processes can be seen from the calculated equilibrium electron densities. Fig. 1 displays the
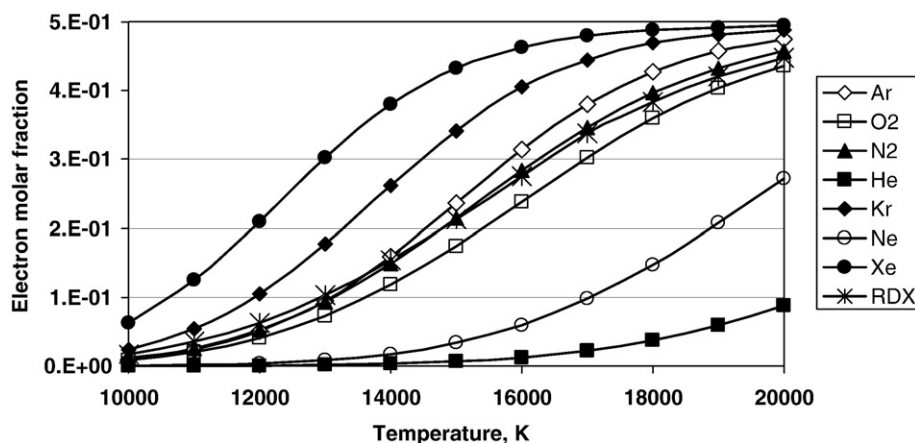

Fig. 1. Temperature dependence of the equilibrium electron density in different buffer gases (5 atm). Calculations were performed with the use of database and program [30].

temperature dependence of the equilibrium electron density calculated for several buffer gases and RDX. Results were obtained for pure gases. The plot demonstrates the electron densities, which may develop within the LIBS plasma plume. Calculations were conducted with the use of a database and program [30]. The highest equilibrium electron concentration is observed in an atmosphere of xenon, and the lowest equilibrium concentration corresponds to helium. The differences in the electron density in different buffer gases are mainly determined by differences in ionization potentials. Results show that temperature dependence of equilibrium electron concentration for RDX gas resembles the dependence for the electron density in nitrogen. The high levels of electron densities demonstrate that contributions of electron-impact processes are substantial.

3. Results and discussion

Fig. 2 presents the temporal profiles of the concentrations of the main species in the RDX LIBS plume for a typical set of initial conditions. Due to the high initial temperature, thermal reactions lead initially to the formation of metastable and excited atoms, which are ionized in thermal processes. The formation of electrons in thermal processes leads to a further rapid accumulation of ions and electrons through electron-impact ionization processes. For species with high ionization

potential, ionization mainly occurs via electron impact. Atomic carbon has a relatively low ionization potential. The ion C^+ can be produced by electron-impact ionization

$$C + e \rightarrow C^+ + e + e + 266 kcal/mol.$$
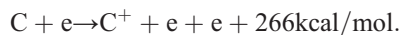
Additionally charge transfer reactions, which take place in the RDX LIBS plume, contribute to C^+ formation,

$$CO^+ + C \rightarrow CO + C^+ - 63 kcal/mol$$

$$NO^+ + C \rightarrow NO + C^+ - 46 kcal/mol$$

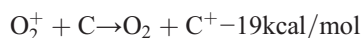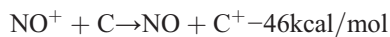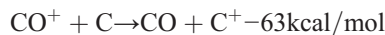$$O_2^+ + C \rightarrow O_2 + C^+ - 19 kcal/mol$$

Fig. 2 contains time dependencies of the concentrations of excited emitting states of oxygen (777 nm) and nitrogen (746 nm) atoms. Reaction pathway analysis demonstrates that the main formation reactions of excited states are electron-impact excitation from the lower electronic states. Electron-impact dissociation of O_2 and N_2 makes a small contribution due to the high degree of dissociation. The main processes removing the excited states are also electron-induced quenching processes. Sensitivity calculations reveal that these excited states are also sensitive to the rate constants of the following reactions of neutral species: $O_2+M=O+O+M$; $OH+M=O+H+M$; $N_2+M=N+N+M$; $N+NO=N_2+O$; $NH+H=N+H_2$; $CN+M=C+N+M$; $NCO+H=NH+CO$; $NCO+O=NO+CO$; $CO+M=C+O+M$. The emission intensities can be calculated by multiplying the concentration of emitting states by the radiative transition probabilities within the framework of our kinetic model.

Kinetic modeling of reactions in the LIBS plume demonstrates that the reaction mechanism can be considered to occur in two stages. In accord with our previous results [4,5] the first stage is characterized by the approach to the quasi-stationary conditions. The high electron concentration sustains high populations of the excited states of H, N and O atoms. The duration of this stage is less than ~ 1 μs. During the second stage, the temperature starts to decrease substantially, and the concentrations of species are in quasi-equilibrium at the decreasing temperature.

Analysis of the two-stage reaction behavior shows that the difference in the mechanisms of initial RDX decomposition is important only during the first reaction stage. Fig. 3 contains the results of calculations for two cases of different decomposition kinetics of RDX: a) gas-phase decomposition of RDX in argon using the decomposition kinetic equation [10], was applied; and b) gas-phase product distribution at the RDX surface under laser irradiation, measured by Fetherolf and Litzinger [11] in argon, was taken as the initial conditions. The results after about 1 μs show very similar reaction behavior. This allows one to simplify the kinetic model for calculations of reaction behavior in the LIBS measurement window (1–30 μs). The results of the analysis of this two-stage reaction behavior suggest, that for modeling of the reaction proceeding in the LIBS measurement window — 1–50 μs, the knowledge of initial reactions of explosive decomposition is not important. As a result of this behavior, the developed model can be used to describe a reaction behavior of
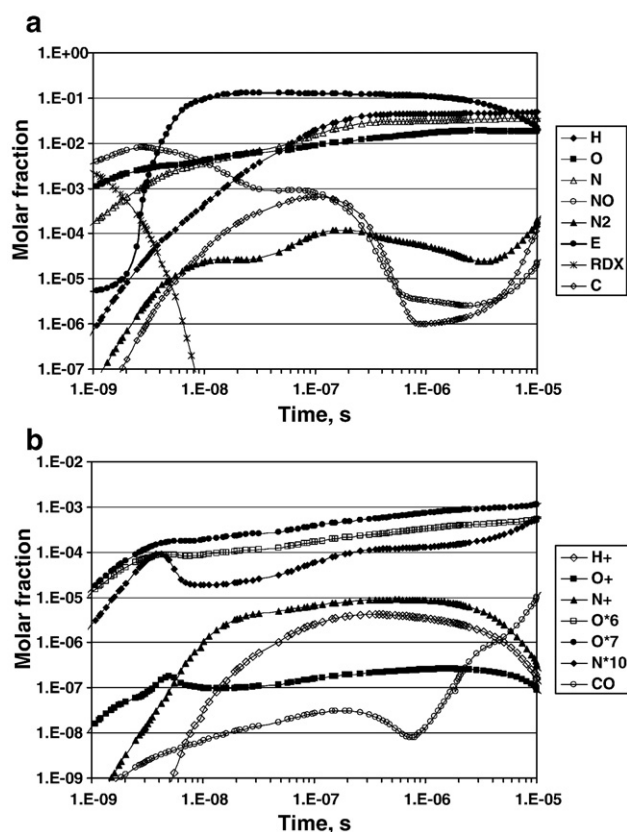

Fig. 2. Time dependence of concentrations of the main species in a plasma plume of RDX (model of initial RDX decomposition [8] with modifications; initial temperature 18,000 K, pressure 10 atm, 1% of RDX in Ar, characteristic temperature quenching time 25 μs).
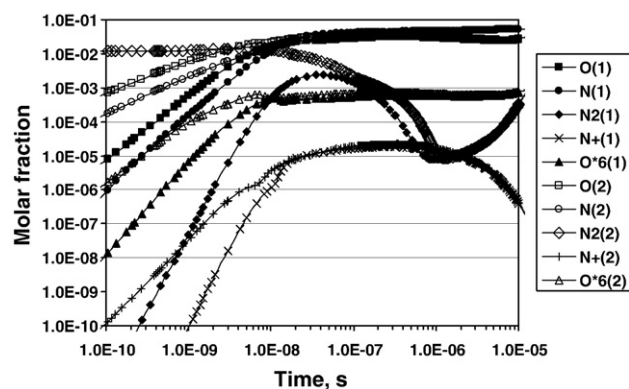
Fig. 3. Time dependence of O, N, N_2, N^+, O*6 (777 nm) concentrations calculated for two models of RDX decomposition: (1) decomposition equation from [10]; (2) the set of gas-phase decomposition products, measured at RDX surface under laser irradiation [11], was taken as the initial mixture composition in Ar (1.38% RDX in Ar, other conditions remain as in Fig. 2).

other C/H/N/O explosives in the gas-phase LIBS plume environment.

Fig. 4 contains results of kinetic calculations of the plasma with four different initial mixtures corresponding to the same N/O/H atomic composition. It demonstrates that a relatively fast approach to approximately the same quasi-stationary state is observed between 10^{-8} and 10^{-7} s. The inclusion of carbon chemistry increases this time (Fig. 3). For the large number of species

considered in the model, quasi-equilibrium is attained at approximately the same times as for the N–O–H system. However several species experience a relatively late approach to quasi-equilibrium at approximately 1 μs (e.g. N_2 and N_2O).

The mechanism of attaining similar mixture compositions for compounds with the same atomic content in the LIBS plume is possibly related to a large difference in the rate constants of radical formation and ionization reactions. To some extent this behavior is the opposite of the two-stage recombination behavior observed experimentally: fast ion recombination with further slower atom/radical recombination. Here fast decomposition processes lead to the formation of the reaction mixture consisting of relatively simple atomic and diatomic atom species mostly during approximately the 10–100 ns period. Because this set of species is approximately the same for initial mixtures with the same atomic composition, this leads to a close reaction states for different mixtures. Further, slower ionization processes and temperature evolution lead to changes in the quasi-stationary state, which is roughly the same for mixtures with the same atomic composition during the time window of LIBS measurements. It means also that quasi-equilibrium or quasi-stationary proceeding is attained at later times than times of attaining approximately the same composition.

It is of interest to note that calculations demonstrate a peak in C_2 species concentrations in the interval between 10 and 400 ns depending on the decomposition rate and temperature decay time
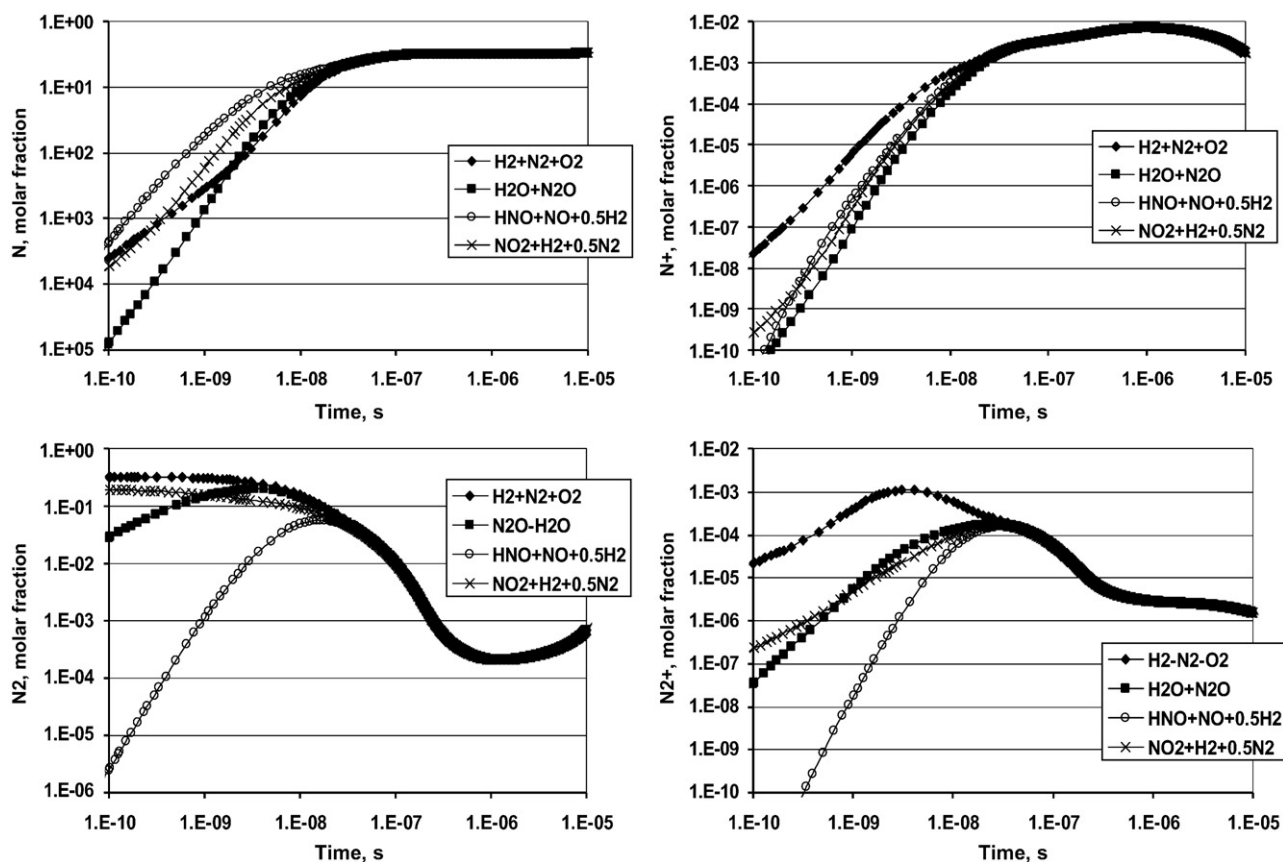

Fig. 4. Results of calculations of N, N^+, N_2 and N_2^+ concentrations for 4 different mixtures with the same atomic composition. Initial mixture compositions are shown on the figure.
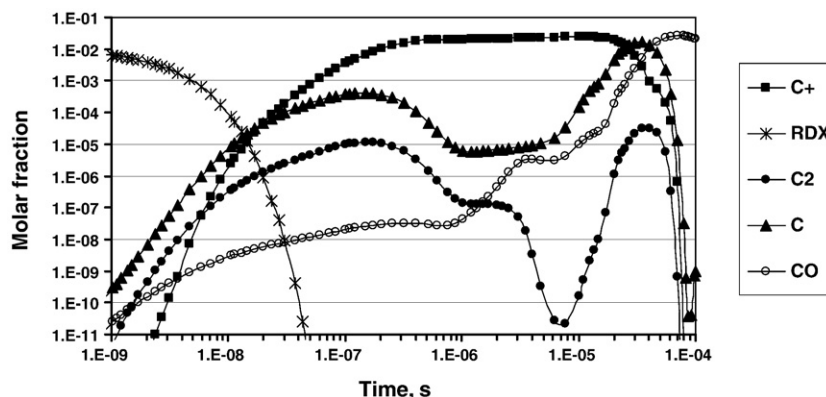
Fig. 5. Double-peak behavior of C_2 concentration (initial temperature 18,000 K, 10 atm, 1% RDX in argon atmosphere).

(Fig. 5). As it was mentioned above, C_2 species were detected in the LIBS plume of different explosives [2]. The temperature decrease during the second stage leads to a further increase in the C_2 concentration and to the appearance of the second maximum. The calculations show that the initial temperature decrease and the increase in quenching rate favor C_2 formation. Initially C_2 is formed mainly in the reactions

$$CO + C \rightarrow C_2 + O + 114 \text{kcal/mol} \qquad (1)$$

$$CN + C \rightarrow C_2 + N + 36 \text{kcal/mol} \qquad (2)$$
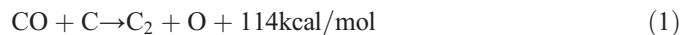
and in recombination processes. The slower dissociation reactions at high temperatures,

$$CN + M \rightarrow C + N + M + 180 \text{kcal/mol}$$

$$C_2 + M \rightarrow C + C + M + 145 \text{kcal/mol},$$
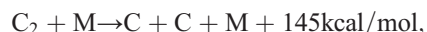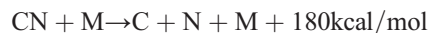
lead to the appearance of the C_2 concentration maximum. A further temperature decrease leads to the substantial decrease in the dissociation rate, the increase of recombination of C+ ions and the increase in the concentration of C_2 that is later consumed in the reactions with radicals.

Harilal et al [35] experimentally observed two peaks in the C_2 concentration during the evolution of laser ablated plasma from a graphite target. They suggested that the first maximum was the result of recombination processes under their experimental conditions. The second maximum was attributed to a dissociation of carbon clusters, leading to the generation of C_2 molecules [35]. Experimental times of the first C_2 peak correspond to the times of modeling results of this work, which are in the 50–300 ns range. The second maximum was experimentally observed in the range 0.5–3 μs. Modeling results show this time is between 10 and 50 μs, depending on initial RDX concentration and characteristic temperature quenching time. Of course, the mechanism of appearance of the two peaks of the C_2 species in laser ablation of graphite may be different. The appearance of second maximum of C_2 species is described by gas-phase reactions in this work.

4. Conclusions

In this work we have developed a kinetic model to describe the processes which lead to the electronically excited states of

oxygen, hydrogen and nitrogen atoms responsible for the emission lines in the LIBS plasma plume of RDX explosive. Kinetic calculations were performed with the use of temperature profiles with the typical decay times in the LIBS plasma. Reaction processes in the RDX plasma were analyzed through kinetic modeling. The main generation reactions of excited states are electron-impact processes. It was found that the evolution of the concentration of C_2 species in the RDX plasma plume demonstrates double-peak behavior. The mechanism of this bimodal C_2 concentration profile was discussed. It is of interest that double-peak behavior of C_2 species was experimentally observed during laser ablation of graphite by Harilal et al. [35]. Experimental times of the observed C_2 peaks approximately correspond to the modeling results.

It was demonstrated that the overall reaction process in the plasma plume can be considered as a two-stage process. In agreement with our previous results (Pb/Ar/air model [4,5]), the first stage corresponds to a fast approach to a quasi-stationary state. The second stage corresponds to a change in the quasi-stationary concentrations of species as a result of the change in temperature. As a result of the two-stage process, the initial composition at the surface of the target, or the initial mechanism of RDX decomposition, is not important in determining the LIBS signature in the LIBS measurement time window. The results of modeling with different mechanisms of decomposition are approximately the same during the second stage. The memory of the initial compound is lost during the period of approximately 1 μs. This allows one to use the suggested model for modeling of the LIBS plume of other C/N/H/O-containing energetic materials in the LIBS measurement window (1–30 μs). Note, that the identification of explosives is possible using their unique ratios of atomic intensities [2].

Acknowledgment

The views and conclusions contained in this paper are those of the authors and should not be interpreted as presenting the official policies or position, either expressed or implied, of the U.S. Army Research Laboratory and National Institute of Standards and Technology or the U.S. Government unless so designated by other authorized documents. Citation of manufacturer's or trade names does not constitute an official endorsement or approval of the use thereof. The U.S. Government has certain rights in copyright of this material.

References

[1] F.C. De Lucia Jr., R.S. Harmon, K.L. McNesby, R.J. Winkel Jr., A.W. Miziolek, Laser-induced breakdown spectroscopy analysis of energetic materials, Appl. Opt. 42 (2003) 6148–6152.

[2] C. Lopez-Moreno, S. Palanco, J.J. Laserna, F.C. DeLucia Jr., A.W. Miziolek, J. Rose, R.A. Walters, A.I. Whitehouse, Test of a stand-off laser-induced breakdown spectroscopy sensor for the detection of explosive residues on solid surfaces, J. Anal. At. Spectrom. 21 (2006) 55–60.

[3] F.C. DeLucia, J.L. Gottfried, C.A. Munson, A.W. Miziolek, Overview of Current US Army Research Laboratory LIBS Security Applications, Abstracts, LIBS—2006, National Research Council of Canada, Montreal, 2006.

[4] V.I. Babushok, F.C. DeLucia Jr., P.J. Dagdigian, M.J. Nusca, A.W. Miziolek, Kinetic modeling of the laser-induced breakdown spectroscopy plume from metallic lead, Appl. Opt. 42 (2003) 5947–5962.

[5] V.I. Babushok, F.C. DeLucia Jr., P.J. Dagdigian, M.J. Nusca, A.W. Miziolek, Experimental and kinetic modeling study of the laser-induced breakdown spectroscopy plume from metallic lead in argon, Spectrochim. Acta Part B 60 (2005) 926–934.

[6] C.F. Melius, in: S.N. Bulusu (Ed.), Chemistry and Physics of Energetic Materials, Kluwer Academic, Netherlands, 1990, pp. 51–78.

[7] N.E. Ermolin, O.P. Korobeinichev, L.V. Kuibida, V.M. Fomin, Study of the kinetics and mechanism of chemical-reactions in hexogene flames, Combust. Explos. Shock Waves 22 (1986) 544–553.

[8] D. Chakraborty, R.P. Muller, S. Dasgupta, W.A. Goddard III, A detailed model for the decomposition of nitramines: RDX and HMX, J. Comput.-Aided Des. 8 (2001) 203–212.

[9] R.A. Yetter, F.L. Dryer, M.T. Allen, J.L. Gatto, Development of gas-phase reaction mechanisms for nitramine combustion, J. Propuls. Power 11 (1995) 683–697.

[10] N.E. Ermolin, V.E. Zarko, Investigation of the properties of a kinetic mechanism describing the chemical structure of RDX flames. I. Role of individual reactions and species, Combust. Explos. Shock Waves 37 (2001) 123–147.

[11] B.L. Fetherolf, T.A. Litzinger, Chemical Structure of the Gas-phase above Deflagrating RDX: Comparison of Experimental Measurements and Model Predictions, 30th JANNAF Combustion Subcommittee Meeting, Monterey, CA, 1993.

[12] Y.-C. Liau, V. Yang, Analysis of RDX monopropellant combustion with 2-phase subsurface reactions, J. Propuls. Power 11 (1995) 729–739.

[13] C. Cavallotti, M. Masi, S. Carra, Modeling plasma-assisted deposition of diamond-like carbon films, J. Electrochem. Soc. 145 (1998) 4332–4341.

[14] G.M. Petrov, J.L. Giuliani, Model of a two-stage rf plasma reactor for SiC deposition, J. Appl. Phys. 90 (2001) 619–636.

[15] T.G. Beuthe, J.-S. Chang, Chemical kinetic modeling of non-equilibrium Ar-CO2 thermal plasmas, Jpn. J. Appl. Phys. 36 (1997) 4997–5002.

[16] T. Kruse, P. Roth, High-temperature reaction of C2 with NO including product channel measurements, Int. J. Chem. Kinet. 31 (1999) 11–21.

[17] T. Kruse, P. Roth, Kinetics of C2 reactions during high-temperature pyrolysis of acetylene, J. Phys. Chem. A 101 (1997) 2138–2146.

[18] Y. Itikawa, A. Ichimura, Cross-sections for collisions of electrons and photons with atomic oxygen, J. Phys. Chem. Ref. Data 19 (1990) 637–651.

[19] S.P. Slinker, R.D. Taylor, A.W. Ali, Electron energy deposition in atomic oxygen, J. Appl. Phys. 63 (1988) 1–10.

[20] S.O. Kastner, A.K. Bhatia, The neutral nitrogen spectrum: term populations, multiplet intensities, diagnostic diagrams, and comparisons with observations, Astrophys. J., Suppl. Ser. 109 (1997) 241–267.

[21] R.M. Frost, P. Awakowicz, H.P. Summers, N.R. Badnell, Calculated cross sections and measured rate coefficients for electron impact excitation of neutral and singly ionized nitrogen, J. Appl. Phys. 84 (1998) 2989–3003.

[22] W. Tsang, R.F. Hampson, Chemical kinetic data base for combustion chemistry. Part I. Methane and related compounds, J. Phys. Chem. Ref. Data 15 (1986) 1087–1279.

[23] M.W. Slack, Kinetics and thermodynamics of the CN molecule. III. Shock tube measurements of CN dissociation rates, J. Chem. Phys. 64 (1976) 228–236.

[24] A. Fontijn, A. Fernandez, A. Ristanovic, M.Y. Randall, J.T. Jankowiak, CO chemiluminiscence and kinetics of the C2+O2 reaction, J. Phys. Chem. A 105 (2001) 3182–3189.

[25] W.E. Wilson Jr., A critical review of the gas-phase reaction kinetics of the hydroxyl radical, J. Phys. Chem. Ref. Data 1 (1972) 535–573.

[26] C. Park, J.T. Howe, R.L. Jaffe, G.V. Candler, Review of chemical-kinetic problems of future NASA missions. 2. Mars entries, J. Thermophys. Heat Transf. 8 (1994) 9–23.

[27] A.R. Fairbairn, The dissociation of carbon monoxide, Proc. R. Soc. Lond. A 312 (1969) 207–227.

[28] H. Tahara, K.-I. Minami, A. Murai, T. Yasui, T. Yoshikawa, Diagnostic experiment and kinetic model analysis of microwave CH4/H2 plasmas for deposition of diamondlike carbon films, Jpn. J. Appl. Phys. 34 (1995) 1972–1979.

[29] M.J. Nusca, M.J. McQuaid, W.A. Anderson, Development and Validation of Multi-species Reacting Flow Model for the Plasma Jet Generated by an ETC Igniter, Proc. 37th JANNAF Combustion Subcommittee Meeting, CPIA Pub.701, vol. 1, November, 2000, pp. 181–191.

[30] L.V. Gurvich, V.S. Iorish, D.V. Chekhovskoi, A.D. Ivanisov, A.Yu. Proskurnev, V.S. Yungman, V.A. Medvedev, I.V. Veits, G.A. Bergman, IVTHANTHERMO — Database on Thermodynamic Properties of Individual Substances, Institute of High Temperatures, Moscow, 1993 (NIST Special Database 5, IVTHANTHERMO-PC, 1998).

[31] R.J. Kee, F.M. Rupley, J.A. Miller, M.E. Coltrin, J.F. Grcar, E. Meeks, H.K. Moffat, A.E. Lutz, G. Dixon-Lewis, M.D. Smooke, J. Warnatz, G.H. Evans, R.S. Larson, R.E. Mitchell, L.R. Petzold, W.C. Reynolds, M. Caracotsios, W.E. Stewart, P. Glarborg, C. Wang, O. Adigun, W.G. Houf, C.P. Chou, C.F. Miller, Chemkin Collection, Release 3.7, Reaction Design, Inc., San Diego, CA, 2002, www.reactiondesign.com.

[32] D.A. Rusak, B.C. Castle, B.W. Smith, J.D. Winefordner, Fundamentals and applications of laser-induced breakdown spectroscopy, Crit. Rev. Anal. Chem. 27 (1997) 257–290.

[33] S. Yalcin, D.R. Crosley, G.P. Smith, G.W. Faris, Influence of ambient conditions on the laser air spark, Appl. Phys. B 68 (1999) 121–130.

[34] R. Krasniker, V. Bulatov, I. Schechter, Study of matrix effects in laser plasma spectroscopy by shock wave propagation, Spectrochim. Acta Part B 56 (2001) 609–618.

[35] S.S. Harilal, R.C. Issac, C.V. Bindhu, V.P.N. Nampoori, C.P.G. Vallabhan, Temporal and spatial evolution of C2 in laser-induced plasma from graphite target, J. Appl. Phys. 80 (1996) 3561–3565.